Highly Aligned Electrospun Nanofibers by Elimination of the Whipping Motion

Pavel Kiselev,[1] Joan Rosell-Llompart[1,2]

[1]*Departament d'Enginyeria Química, Universitat Rovira i Virgili, Avda dels Països Catalans 26, 43007 Tarragona, Spain*
[2]*ICREA (Catalan Institution for Research and Advanced Studies), Barcelona, Spain*

Received 26 August 2011; accepted 16 November 2011
DOI 10.1002/app.36519
Published online 22 January 2012 in Wiley Online Library (wileyonlinelibrary.com).

ABSTRACT: This work shows how elimination of the whipping motion of electrospinning fibers leads to nearly perfect alignment of fibers collected onto fast-rotating cylindrical collectors. The whipping motion is eliminated by using lower and more uniform electrical fields than are typically used in electrospinning practice and by pulling the fiber mechanically by the collector. Two types of polymeric fibers, solid fibers of poly(ethylene oxide) and porous fibers of polystyrene, are collected at collector surface speeds ranging from 2 to 15 m/s, showing a rapid transition from either nonaligned or wavy fibers, to straight fibers with nearly perfect alignment (over 95% of the fibers within 1° and 100% within 4°). Very high collection speeds lead to worsening of alignment, apparently because of air turbulence created by the cylinder rotation. The degree of fiber stretching is quantified as a function of the collector surface speed. A 50% decrease in average diameter is measured for PEO fibers, while for porous PS fibers; it decreases by <30% over the same range in collection speed. © 2012 Wiley Periodicals, Inc. J Appl Polym Sci 125: 2433–2441, 2012

Key words: electrospinning; aligned fibers; whipping; bending instability

INTRODUCTION

Electrospinning is a fast-developing method for production of polymeric and composite fibers with diameters ranging from few micrometers down to tens of nanometers. High charge density on the electrospun jet leads to extensive stretching, which is responsible for such small final diameters, and also believed to be responsible for the unstable trajectory and development of semichaotic motion called whipping (or bending) instability. This motion is commonly observed in electrospinning experiments and, therefore, typical electrospun deposits are nonwoven mats of randomly oriented fibers. However, for some applications, it is important that nanofibers form ordered arrays rather than random mats.[1–3] Materials made with uniaxially aligned electrospun fibers have anisotropic characteristics (mechanical, physical, etc) which are useful in diverse applications, such as suture threads,[4] sensors,[5] vascular scaffolds,[6,7] scaffolds for wound repair,[8] biomimetic extracellular matrices,[9] anisotropic wetting, and membranes for fuel cells.[10]

Fiber alignment has been achieved by different approaches: (i) by electrostatic steering of the fiber at the collector (either actively, by means of electrodes,[11,12] or spontaneously, by collecting the fibers onto frames or wire assemblies[13]), (ii) by mechanical means, winding the fiber over a rapidly moving collection surface,[2] such as a rotating cylinder[14–16] (also called "drum" or "mandrel") or the edge of a rotating disc or wheel,[7,17–19] and (iii) by a combination of mechanical and electrostatic means.[20–22]

Collecting on a rotating cylinder allows coverage of comparatively large surface areas, but obtaining highly aligned fibers on rotating cylinders has been challenging. To obtain straight aligned fibers by this method it is necessary for the collector surface speed to match or exceed the rate at which fiber is produced (typically, several m/s); otherwise, the fiber assumes different orientations on the collector or buckles upon deposition. Varying degrees of success have been reported, however. In a few works, poor alignment achieved by a rotating collector method can be attributed to a low collection speed, insufficient to exceed the rate at which fiber was produced.[23] In other studies, alignment was rather poor, despite using very high collection speeds (9.5–33.5 m/s).[24–27] Only in one

Correspondence to: J. Rosell-Llompart (joan.rosell@urv.cat).
Contract grant sponsor: European Commission (Marie Curie program); contract grant number: MTKD-CT-2005-030040.
Contract grant sponsor: Spanish Ministry of Science and Innovation; contract grant numbers: CTQ2008-05758/PPQ, CIT-420000-2008-30.
Contract grant sponsor: Catalonian Government; contract grant number: 2009-SGR-1529.

instance[15] was the alignment very good (within $<\pm 1^\circ$). A combination of rotating collectors and auxiliary electrodes has produced better results than without electrodes.[20,21] Apparently, this lack of consistent or successful results has led one review to conclude that it is difficult to fabricate highly aligned fiber assemblies using rotating cylinders, and that fiber breakages may occur if the rotating speed is too high.[2]

Our goal in this study is to investigate whether the rotating cylinder method can be used to eliminate the random jet motion, to achieve very high fiber alignment consistently. By use of a low electric field near the tip of the needle and at low liquid flow rate, we are able to produce single filament electrospinning steadily. These conditions avoid multiple jetting (multijetting), as well as liquid accumulation at the needle tip (the latter being frequently met in the practice of this art). In addition, by means of an electrode plate positioned behind the electrospinning emitter, a more uniform field is created that greatly suppresses the whipping instability. These well-defined electrospinning conditions allow us to produce continuous fibers of poly(ethylene oxide) (PEO) and of polystyrene (PS), for which we quantify the degree of fiber alignment and of stretching as a function of collection conditions (collector speed and radius). In addition, we determine whether the pulling by the cylinder causes fiber breakages, such as those reported for PEO fibers collected on the edge of a wheel.[18]

EXPERIMENTAL

Materials

PEO (M_v = 600,000, ρ_{PEO} = 1.21 g/cm^3), PS (M_w = 350,000, M_n = 170,000, and ρ_{PS} = 1.04 g/cm^3), and ACS grade solvents were purchased from Sigma-Aldrich and used without further purification. Water was purified in a Milli-Q water deionizer (Millipore). PEO solutions 6% wt/wt were prepared at room temperature by slow addition of PEO to the 1 : 1 v/v water : ethanol mixture under constant stirring. PS solution 20% wt/wt were prepared by dissolving PS in *N*,*N*-dimethylformamide (DMF) while stirring. After preparation the solutions were stored at room temperature. The densities of these solutions (ρ_{sol}) were determined to be 0.94 ± 0.01 g/cm^3 for 6% PEO solution and 0.97 ± 0.01 g/cm^3 for 20% PS solution. The PEO solution was not clear, while the PS solution was transparent.

Electrospinning

A schematic diagram of the electrospinning arrangement with a rotating collector is shown in Figure 1(a). A syringe pump (KDS 100-CE) was used to generate liquid flow. PEO fibers were spun at a solution flow rate of 25 μL/h from a 26 GA stainless steel needle (Hamilton RN-needle, 460 μm OD, and 260 μm ID), which was square terminated and was fitted to a glass syringe. PS solutions were spun at flow rate of 50 μL/h from the needle assembly shown in Figure 1(b), which provided vapor-laden sheath gas around the solution meniscus at the needle tip to prevent polymer solidification. The needle in this case was a polyimide-coated fused silica capillary (200 μm OD and 100 μm ID), which was passed through a tee and was centered in a glass capillary (ID = 0.7 mm) from which the needle protruded by 1 mm. Nitrogen gas containing DMF vapor flowed through the tee to create a sheath flow around the silica capillary of 50 cc/min (linear exit gas velocity near needle ~ 240 cm/s). Positive high voltage from a HV power supply (Ultravolt HV-RACK-4-250-00228) was applied to the syringe needle in the configuration of Figure 1(a), and to the solution upstream from the silica capillary in Figure 1(b). An additional electrode ("back electrode"), a 10 × 10 cm^2 square brass plate with a small hole in the middle, was typically used. It was placed 30 and 20 mm behind the needle end, as shown in Figures 1(a,b), respectively. This back electrode was connected to the same high voltage as the needle/solution.

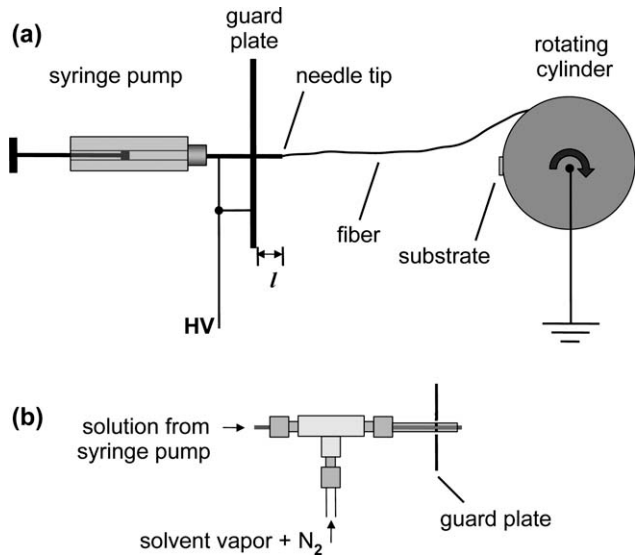

Figure 1 (a) Experimental arrangement for electrospinning without sheath gas flow (HV = high voltage) and (b) modified needle used with sheath gas flow for PS solution. Back electrode is labeled "guard plate." Not drawn to scale.

In some tests, fibers were collected on a grounded metal plate ("stationary target"). More typically, the collector was an electrically grounded spinning aluminum cylinder, of length equal to 18 cm, and placed orthogonal to the needle at a separation of 10.5 cm for PEO and 15.5 cm for PS. With larger separation the

amplitude of fiber whipping increases. The chosen distances are just large enough to allow sufficient drying of the fibers before reaching the collector. Cylinder rotation speed could be varied from 1100 to 4000 RPM, and was measured with a tachometer (Sentry ST722). Three cylinder diameters were used, $D_C = 3$, 5, and 7 cm. The tachometer readings (RPM) were used to compute the linear speed of the collector surface, later referred to as "take-up speed" or "collector surface speed," according to v_C (m/s) = RPM $\times \pi \times D_C$ (cm)/6000.

Conditions were adjusted to produce a single continuous fiber. Needle voltage was carefully selected to ensure no accumulation of liquid at the meniscus, and it was found to vary slightly for the different collectors and solutions used: 9.0 kV for PEO, and, for PS, 11.4 kV for data set (a) and 9.5 kV for data set (b). Before sample collection on a cylinder, the electrospinning process was allowed to reach steady state with the stationary target placed in front of the cylinder; after which time, the target was removed and collection on the rotating cylinder started. Relative humidity varied within 40–60% RH, and room temperature was within 21–23°C.

Fiber collection and sizing

Fibers for imaging were collected on rectangular 0.5 mm thick silicon wafer substrates of $\sim 12 \times 4$ mm^2 size, for 1–2 min. One or several substrates were attached using double-sided tape to the cylinder, with their long side parallel to the cylinder axis, or to the stationary target. The electrical insulation provided by the tape was insufficient to cause any charge accumulation resulting in electrostatic repulsion of incoming fibers. All samples within each data set were collected without interrupting the electrospinning process.

Fibers were imaged by optical microscopy (Kyowa ME-LUX2) and by scanning electron microscopy (FEI Quanta 600 FE-SEM). The fiber diameters and the fiber angles of each experimental condition were determined from multiple SEM images from the same wafer. Each sample comprised around 40 fibers, and the image resolution for fiber diameter determination was such that the fiber width would span at least 15 pixels for the thinnest fiber, and between 30 and 60 pixels for most fibers.

RESULTS AND DISCUSSION

A back electrode[28–30] was used in combination with a rotating cylinder for production and collection of polymer fibers. This electrode geometry helps create a uniform electrical field between the needle and the collector, which has several practical advantages. It gives better control over the deposition of the fibers by greatly reducing the influence from nearby objects (such as light sources or electrical cables) and by directing the fiber straight towards the collector. It also reduces or even eliminates the bending instability responsible for fiber whipping, thus restricting fiber deposition to a much smaller area. The degree by which the bending instability is suppressed for a given solution and distance to the substrate depends mostly on the length l by which the needle protrudes from the back electrode [Fig. 1(a)], as well as on the electrode size. Because the addition of a back electrode at constant voltage reduces electric field strength at the needle end, the voltage supplied to the needle had to be increased to maintain electrospinning. For reference, the minimum voltage for stable electrospinning of the PEO solution was around 9–10 kV with a back electrode, while without it 5 kV was sufficient to produce a stable electrospinning with the same electrical current measured on the collector, although the mean field strength between the needle and collector is larger with back electrode. To sum up, 9–10 kV used in our configuration with back electrode is comparable to around 5 kV in a more typical apparatus (without back electrode).

PEO fibers

For our PEO solution, fiber whipping happened only in the absence of the back electrode. With the back electrode, whipping was completely suppressed for the whole fiber length between the needle and the stationary target. In this case, the fiber traveled in a straight line to a point on the collector, and the point of deposition slowly drifted about so that the area of fiber deposition was slowly growing in time from an initial tiny spot to a circle a few millimeters in diameter after prolonged deposition. When a rotating cylinder was used, no whipping was observed either, although a slight fiber motion near the collector was induced, possibly, by the air flow caused by the cylinder rotation. The collected fibers were always aligned in the direction of cylinder rotation, although they were not necessarily straight. At low collection speeds, they were coiled or wavy due to buckling upon impacting on the collector surface, as shown in Figure 2(a), which shows predominantly wavy fibers, mixed with some coiled and some straight (linear) ones. At higher speeds, the fibers became straight [Fig. 2(b,c)]. At the intermediate collection speed of Figure 2(b), the predominant fiber shape was straight, but about a 10th of them was wavy, although no coiled fibers were found. Straightening of the fibers is expected to begin when the collector surface speed v_C approaches the fiber production rate, FPR, which we define as the length of fiber collected per unit time

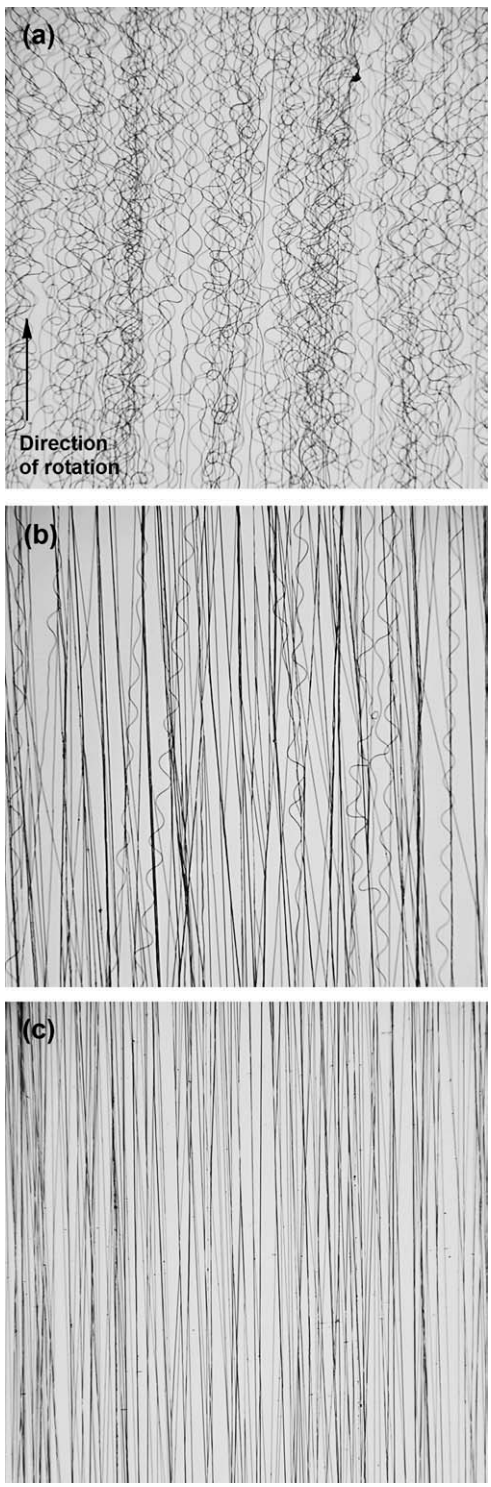

Figure 2 Optical images of PEO fibers collected on 3 cm cylinder at different collector surface speeds: (a) 2.07; (b) 3.53; (c) 4.71 m/s.

on a stationary target under otherwise similar experimental conditions as with the rotating collector. When v_C exceeds FPR, the collected fiber is expected to become straight, and either stretch or break. The presence of both straight and wavy fibers at 3.53 m/s [Fig. 2(b)] suggests that v_C is near FPR, and can be explained by variability in FPR or v_C. The small variability in fiber angle observed in Figure 2(c) may be caused by small amplitude whipping or side motions of the airborne fiber, or by unsteady tugging of the fiber by the rotating cylinder.

Increasing the rotational speed of the cylinder caused a decrease in fiber diameter, for high enough speeds, as expected. Figure 3 shows the quadratic mean fiber diameter versus cylinder surface speed for the three different cylinder diameters used, along with ± 1 standard deviation bars. The agreement between the three data sets shows that the cylinder size does not influence the PEO fiber diameter. Fiber thinning has previously been reported[31,32] and is obviously the result of stretching associated with the pulling of the fiber by the collector. When $v_C \geq$ FPR the deposited fibers are straight and aligned in the direction of rotation. In this case, the rate of fiber length collected on the cylinder should be very close or equal to v_C, and the quadratic mean fiber diameter can be predicted from mass balance[33] by relating the total weight of the collected fibers with the infused volume of polymer solution:

$$D = 2\sqrt{\frac{QC\rho_{\text{sol}}}{\pi v_C \rho_f}} \tag{1}$$

where Q is the volumetric flow rate of the polymer solution, C the polymer weight fraction in the solution, ρ_{sol} is the solution density, and ρ_f is the density of the collected dry fiber. The quadratic mean of each sample is computed as

$$D = \sqrt{\sum d_i^2/N} \tag{2}$$

where d_i ($i = 1, 2, \ldots N$) are the experimental fiber diameter values, and N is the number of measured

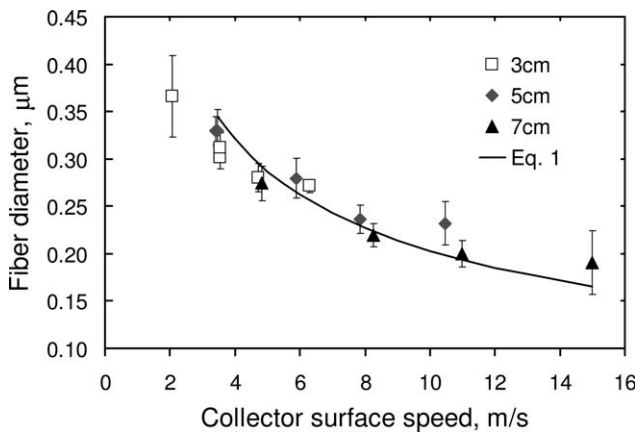

Figure 3 Average PEO fiber diameter (quadratic mean) versus collector surface speed, for different cylinder diameters. Solid line is from eq. (1). Bars represent ± 1 standard deviation.

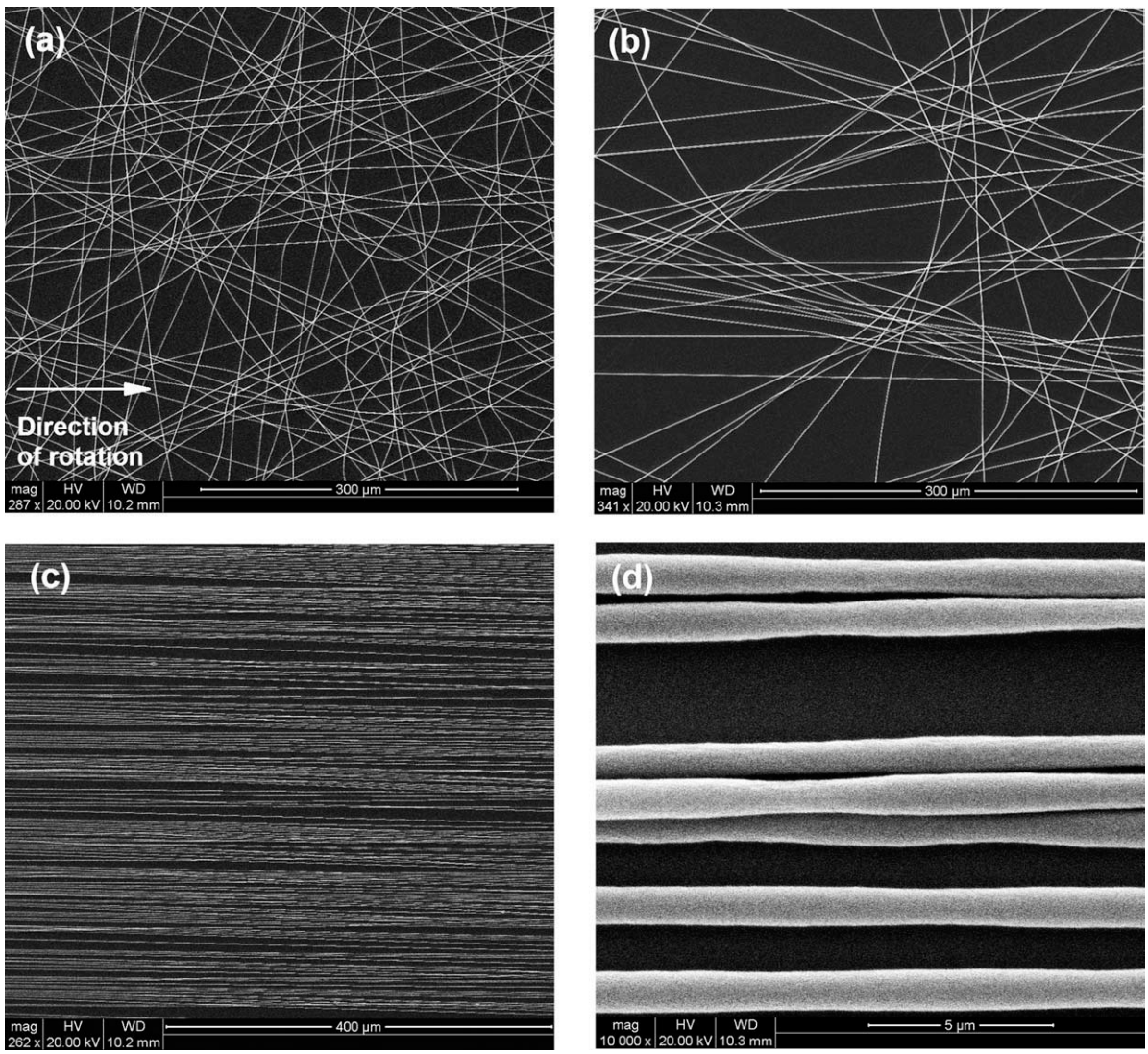

Figure 4 SEM images of PS fibers collected at different collector surface speeds: (a) 2.0; (b) 3.3; (c) 6.5; (d) 6.4 m/s. Fiber "necking" is shown in (d). Cylinder diameter: 3 cm for (a) and (d); 5 cm for (b) and (c).

fiber diameter values in a sample. The quadratic mean diameter is chosen instead of the usual count mean diameter, because it is directly comparable to the average fiber size predicted based on mass conservation.

The diameter predicted from eq. (1) versus the collector surface speed, v_C, is represented in Figure 3 by a solid line, and is in good agreement with the experimental PEO fiber diameters in the range of speeds corresponding to straight fibers (>4 m/s). For speeds under 4 m/s, for which FPR apparently exceeds the collector linear speed, as indicated by the buckling of the fibers on the stationary target (Fig. 2), eq. (1) overestimates the experimental values.

The following picture emerges from these data and observations. At sufficiently low linear surface speeds of the collector (under $\sim$ 3 m/s), the electrospinning of PEO solution is not apparently affected by the rotation of the cylinder, and the PEO fiber buckles as it impacts onto the collector surface, leading to aligned coiled and wavy fibers. At higher cylinder speeds, the mechanical pull by the cylinder on the fiber propagates upstream along the fiber length, causing the straightening the fiber with little change in diameter at the lower speeds ($\sim$ 4 m/s), and, at high enough speeds (exceeding 4 m/s), causing significant stretching and thinning.

PS fibers

The PS solutions in various solvents were found to be difficult to electrospin with the unsheathed needle [Fig. 1(a)] due to solidification of the meniscus right outside the needle tip. It was possible to electrospin PS in DMF, but the resulting fibers varied greatly in diameter and many broken ends were observed. As shown by Larsen et al.,[34] a sheath flow of solvent vapors around the liquid meniscus helps

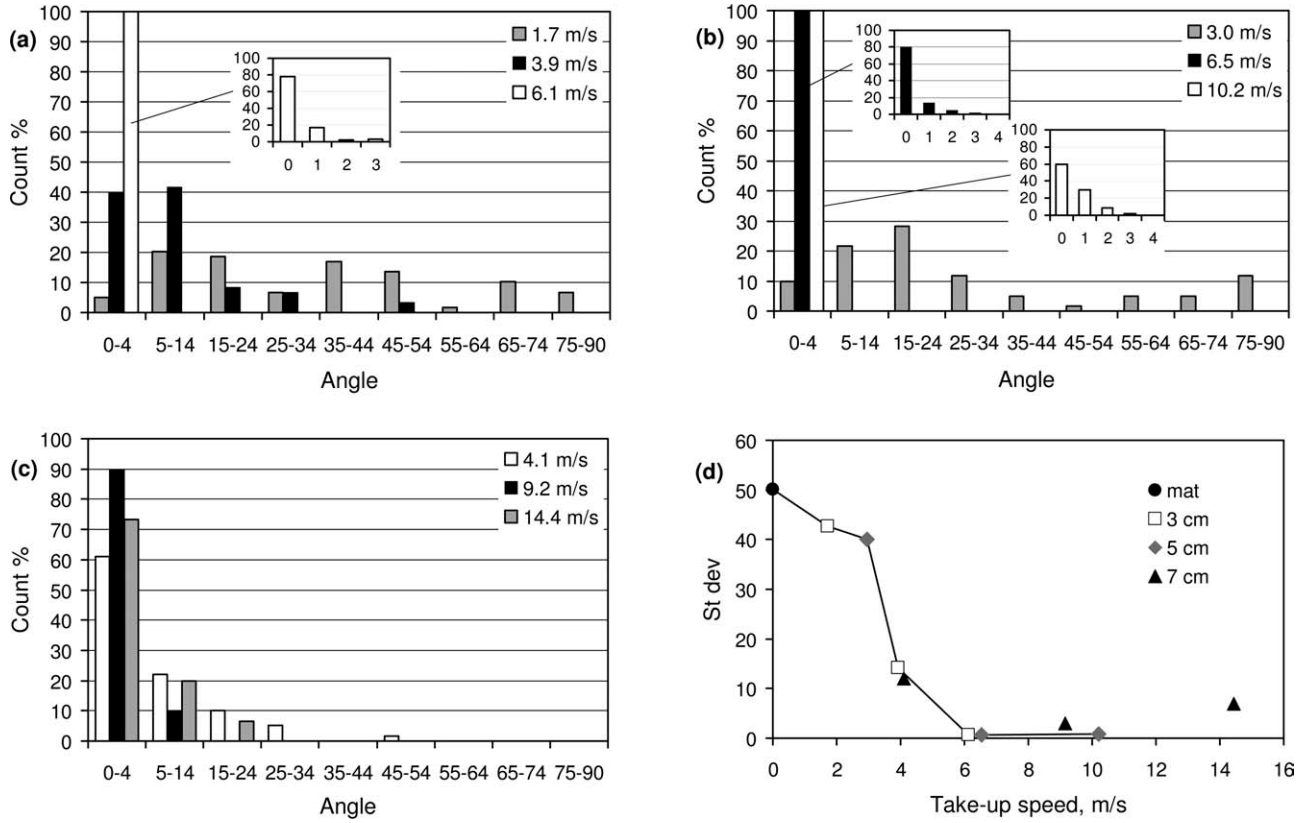

Figure 5 Histograms of PS fiber angle distributions relative to mean orientation (angle = 0°) for cylinder diameters (a) 3, (b) 5, and (c) 7 cm; and (d) standard deviation from these distributions against collector surface speed. Insets in (a) and (b) expand the narrowest distributions. The line in (d) connects the points for the 3 and 5 cm cylinders to guide the eye. (d) Includes a point at "zero" collector speed for fibers collected onto the stationary target as a random mat.

to protect it from the surrounding laboratory air, which sometimes can cause drying in that area. However, the solvent we use, DMF, has a low volatility (b.p. = 153°C) and drying is unlikely be the main cause of solidification of the solution. We hypothesized that the solidification was caused by the interaction of the solution with humidity in the ambient air, which will be explained later, so the sheathed needle was implemented to shield the meniscus from the ambient air [Fig. 1(b)]. With it, the PS fibers became continuous and much less variable in size. In contrast with the PEO case, the whipping instability for the PS solution was not suppressed completely by the presence of the back electrode (with or without sheath gas). Since the electrode configuration and voltage and, therefore, the electrical field in both cases was very similar, the degree of suppression of whipping must depend on the solution properties as well.

With the back electrode, the fibers were collected on the stationary target as randomly oriented fibers within a circular mat about 5 cm in diameter, for a needle-collector distance of 15.5 cm. On a rotating cylinder at low take-up speeds the fibers were also randomly oriented, as shown in Figure 4(a) for 2 m/s. At increased take-up speeds, the PS fibers became more ordered [Fig. 4(b)], until the alignment was nearly perfect [Fig. 4(c)] at around 6 m/s. Necking along the fiber, that is, variation of fiber thickness, was observed at take-up speeds above 6 m/s [Fig. 4(d)].

The fiber angle distributions obtained with the three cylinders at different take-up speeds are shown in Figure 5(a–c). The fiber angle (0–90°) is defined as the angle between the fiber and the mean fiber direction (i.e., the direction of winding on the cylinder). For the two smaller cylinders [Fig. 5(a,b)], almost perfectly aligned fibers were obtained for speeds in the range 6–10 m/s, with more than 99% of the fibers within <4° from the mean fiber direction, and more than 95% of the fibers within an angle spread of <1° from the mean fiber direction. With the largest cylinder [Fig. 5(c)], however, we did not obtain such high degree of alignment, and alignment worsened significantly on increasing speed from 9.2 to 14.4 m/s.

The standard deviations of these angle distributions are graphed versus cylinder take-up speed in Figure 5(d). The graph includes a point at "zero" collector speed for fibers collected as a random mat onto the stationary target. The transition from random (large Stdev) to aligned fiber orientations (small

Stdev) starts rather sharply between 3 and 4 m/s. There is good agreement between all data sets for speeds under 7 m/s, and the best alignments (smallest Stdev) occurred for take up speeds between 6 and 7 m/s. At higher speeds, the alignment worsened with increasing take-up speed, becoming notably worse with the 7 cm cylinder than with the 5 cm cylinder. Under the conditions of best alignment with the 3 and 5 cm cylinders (at take-up speeds around 6 m/s), the whipping instability was sometimes completely eliminated, and other times it developed 3–5 cm downstream from the needle, initially growing in amplitude, then diminishing until the fiber followed a straight path in the last few centimeters before the collector. With the 7 cm cylinder, on the other hand, the fiber motion was visibly more chaotic under similar take-up speeds (4–9 m/s), and became even more so at higher speeds, above 9 m/s. This behavior is indicative of turbulent airflow. The Reynolds number ($\mathrm{Re} = v_C D_C/\nu_{\mathrm{air}}$) computed for the 7 cm cylinder ($D_C = 0.07$ m) at $v_C = 9.2$ m/s, $\mathrm{Re} = 4.1 \times 10^4$, is consistent with turbulent flow caused by the cylinder rotation.[35] In addition, in our system, turbulence may have been enhanced by cylinder vibration, or locally by the silicon substrate attached to the cylinder.

Figure 6(a) shows the dependence of fiber diameter on the take-up speed for the samples of Figure 5, and includes a zero speed value from fibers collected onto the stationary target. At low speeds, the diameter remains constant until past 4 m/s, at which the fibers have already become significantly aligned [Fig. 5(d)]. Beyond 4–5 m/s, the fiber diameter decreases with increasing take-up speed, but not nearly as fast as expected from mass balance (solid line) assuming that the fiber density in eq. (1) equals that of the bulk polymer [Fig. 6(a)]. This observation was confirmed with a second data set, shown in Figure 6(b). In both data sets, the standard deviations of the diameter distribution (bars) were much larger for the 7 cm cylinder than for the other cylinders. This cylinder size also led to the largest deviations from the theoretical curves (solid lines).

Hypothetically, the difference in Figure 6(a,b) between experimental and theoretical fiber diameter (symbols and solid lines) could be due to either of the following reasons: (i) the fiber being discontinuous (broken), (ii) a noncircular cross section of the fibers (flattened on the plane of the SEM images), or (iii) a lower density of the fiber compared to the bulk polymer. The first two possibilities were dismissed from optical and SEM images of collected fibers, as no loose ends were observed and the fibers appeared to be perfectly circular [Fig. 7(a)]. However, a porous internal structure with formation of a skin has been reported previously for PS fibers produced from DMF solutions at relative humidity of

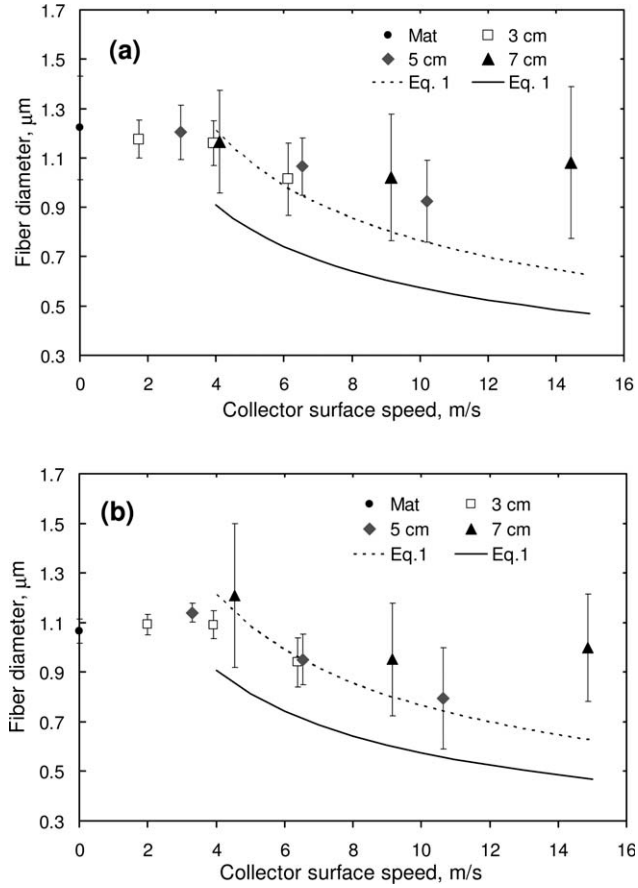

Figure 6 Average PS fiber diameter (quadratic mean) versus collector surface speed, for different cylinder diameters, from two independent sets: (a) and (b). Solid and dashed lines are from eq. (1). Solid lines assume a fiber density equal to the bulk density of PS ($\rho_f = \rho_{PS}$). Dashed lines take into account fiber porosity ($\rho_f = 0.75^2\ \rho_{PS}$). Bars represent ±1 standard deviation.

24% and higher.[36] The porous nature of our fibers can be appreciated in the example of Figure 7(b), which was produced by breaking a silicon wafer substrate covered with fibers, and shows cross sections of two fibers of different diameters. This porous structure is comparable to Pai et al. Figure 6(a)[36] and Demir's Figure 3(a).[37] To determine the degree of porosity, new PS fibers were collected and were annealed at 100°C for 2 h. This temperature was chosen at a few degrees above the glass transition temperature for this polymer ($T_g = 95$°C, as reported by the supplier). In three samples, the annealing caused fiber shrinkage to 75% of the initial fiber diameter, on average (Table I). Therefore, the theoretical prediction in Figure 6(a,b) was recalculated from eq. (1) assuming a fiber density equal to 0.5625 ($= 0.75^2$) of the bulk density of PS. This prediction (dashed lines) is now in fairly good agreement with the experimental data for aligned fibers at speeds between 4 and 8 m/s, while at speeds beyond 8 m/s it significantly underestimates

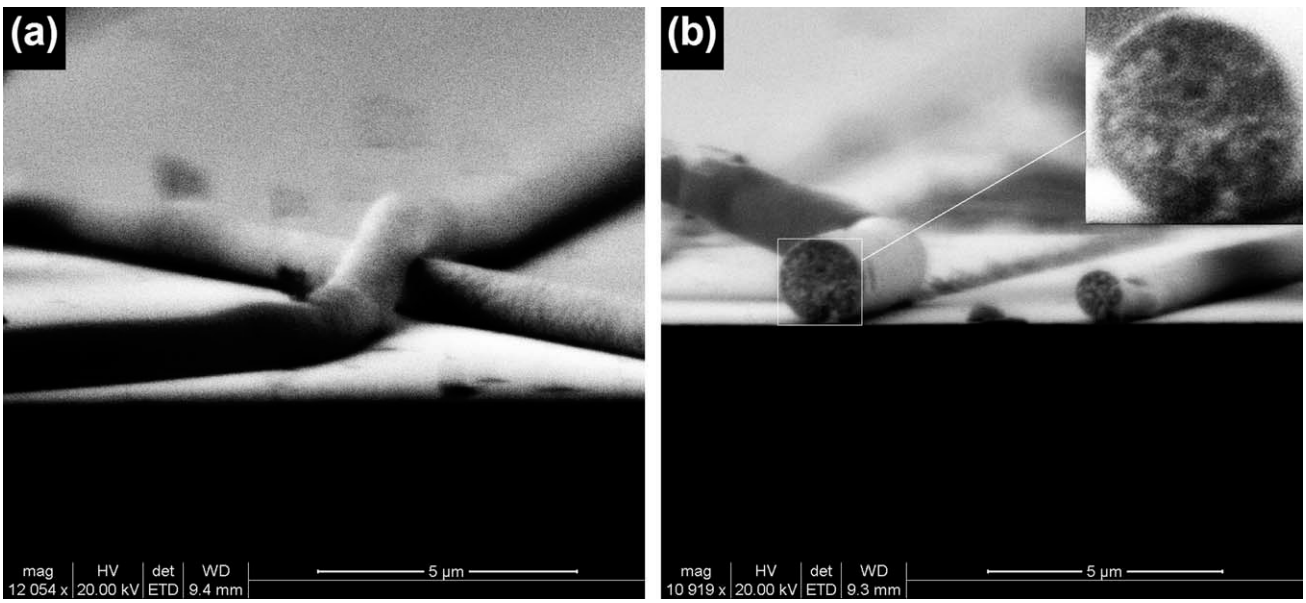

Figure 7 Side views of PS fibers collected on the stationary target at 30% ambient humidity, revealing circular cross section, and porous internal structure.

the 7 cm data in both sets (especially at the highest collector speed) and the 5 cm datum in Figure 6(a).

In conclusion, even though the sheath flow was present, it did not shield the fiber from the ambient air some distance away from the needle, and the porosity of PS fibers is explained by precipitation of the polymer due to the antisolvent effect of water present as vapor in the ambient air. Interestingly, some of the thicker than expected fibers of the 7 cm cylinder data shown in the two independent sets of Figure 6(a,b), as well as the larger standard deviations for this cylinder, are consistent with enhanced water vapor transport to the fiber, caused by the greater turbulent airflow expected for this cylinder size. Enhanced vapor transport would have caused precipitation of PS at earlier stages of fiber formation, where the fiber is thicker, resulting in thicker, more porous fibers on the collector.

The FPR estimate can be obtained from the stretching and alignment data. Assuming that there is no significant stretching during the alignment of fibers, the FPR would be close to the lowest collection speed at which good alignment is reached. For the PS fibers formed in our experiment, it must lie between 4.0 and 6.1 m/s, because at 4.0 m/s there is no stretching and the alignment is still poor, while at 6.1 m/s alignment is already nearly perfect while some degree of stretching occurs [Figs. 5(d) and 6(a,b)].

To our knowledge, only a few reports come close to the high degree of fiber alignment obtained in the current study.[15,20,21] Two of the studies use unusual electrode configurations aimed at focusing the fibers toward a particular region on the collection cylinder. Sundaray et al.[20] positioned a steel pin counter-electrode beside an insulating rotating cylinder, while using a small inter-electrode separation (2.2 cm) and collection speed of 4.2 m/s and a voltage of 4.8 kV. Tong and Wang[21] fit a conducting cylinder with a set of posterior knife edge bars.[21] In this case, a larger interelectrode separation (10 cm) was used, and at the highest take-up speed tested (6.3 m/s), more than 90% of the fibers were within $\pm 4.5^\circ$ of mean orientation. Only in two studies[15,16] high alignment was achieved solely by mechanical pull of a conducting rotating cylinder for different polymers from those in this study (a copolymer of ε-caprolactone and ethyl ethylene phosphate, and polyvinylbutyral). The factors leading to this high alignment were not studied in these works; however, it is worth noting that they both used a low field, as in our study (5 kV). It is obvious that random motion near the collector (such as induced by whipping) must be eliminated either by electrostatic control or by mechanical pulling to achieve good fiber alignment. At low field, whipping is already reduced making its elimination easier. In our case,

TABLE I
Fiber Diameters Before and After Fiber Annealing from New Samples Collected on the 5 cm Cylinder at 40–50% RH

Cylinder surface speed (m/s)	Before annealing (µm)	After annealing (µm)	Diameter ratio
3.25	0.943 (±0.050)	0.706 (±0.046)	0.75
6.54	0.938 (±0.057)	0.731 (±0.056)	0.78
10.6	0.931 (±0.046)	0.675 (±0.046)	0.72

In brackets: ±1 standard deviation.

the back electrode has probably played a significant role in getting aligned fibers because it strongly suppresses whipping. Conversely, many electrospinning experiments use very high fields, creating multiple jets and intense whipping, which would be more difficult to suppress with a back electrode, even at very high rotation speeds.[24,25,27,31,32]

CONCLUSIONS

The effects of mechanical drawing of electrospun fibers by rotating cylindrical collectors have been studied for linear collection speeds up to 15 m/s under conditions of steady-state single-fiber electrospinning, for two different polymer-solvent systems: PEO/water-ethanol and PS/DMF. It was found that the whipping instability is suppressed by means of a back electrode. PEO fibers followed a straight path at any collector take up speed (or even onto a stationary collector), while for PS eliminating whipping required the assistance of the mechanical pull from the rotating collector. The elimination of whipping lead to very high alignment of collected fibers.

A transition from nonstraight fibers (aligned, coiled and wavy, for PEO, and randomly oriented for PS) to aligned and straight fibers was observed with increasing collector surface speed. This transition happened at $\sim$ 3.5 m/s for PEO and between 4.0 and 6.1 m/s for PS. We interpret these values to be near the Fiber Production Rate, FPR, which is defined as the fiber length that would be collected on a stationary target per unit time. At collector speed beyond FPR, fibers were stretched and their diameters decreased without breakages. For PEO, this decrease agreed well with the prediction from mass balance, while for PS it did only after the fiber low density arising from porosity is taken into account. Porous PS fibers presumably formed by precipitation due to absorbed water vapor, which acts as antisolvent. The fibers from PS solution developed necking at collection speeds above $\sim$ 6 m/s, but neither PEO nor PS fibers showed any breakages or the neck and fibrillar structures reported by Zussman et al.,[18] despite much higher collection speeds used in this study (up to 15.0 m/s).

The best alignment for PS fibers was quantified to be within 4° of the mean direction for 100% of the fibers, and within 1° for 95% of the fibers. Compared with the smaller cylinders (3 and 5 cm in diameter), the 7 cm collector led to reduced alignment, as well as thicker fibers with more variation in their width. We attribute these differences to air turbulence (expected for the larger Reynolds numbers with the larger cylinder), which presumably perturbs the fiber path and enhances the transport of water vapor to the fiber, promoting solidification of the fiber earlier in the fiber path.

References

1. Huang, Z. M.; Zhang, Y. Z.; Kotaki, M.; Ramakrishna, S. Compos Sci Technol 2003, 63, 2223.
2. Teo, W. E.; Ramakrishna, S. Nanotechnology 2006, 17, R89.
3. Park, S.; Park, K.; Yoon, H.; Son, J.; Min, T.; Kim, G. Polym Int 2007, 56, 1361.
4. He, C. L.; Huang, Z. M.; Han, X. J. J Biomed Mater Res 2009, 89A, 80.
5. Kessick, R.; Tepper, G. Sens Actuators B 2006, 117, 205.
6. McClure, M. J.; Sell, S. A.; Ayres, C. E.; Simpson, D. G.; Bowlin, G. L. Biomed Mater 2009, 4.
7. Xu, C. Y.; Inai, R.; Kotaki, M.; Ramakrishna, S. Biomaterials 2004, 25, 877.
8. Liu, Y.; Ji, Y.; Ghosh, K.; Clark, R. A. F.; Huang, L.; Rafailovichz, M. H. J Biomed Mater Res 2009, 90A, 1092.
9. Chen, F.; Su, Y.; Mo, X. M.; He, C. L.; Wang, H. S.; Ikada, Y. J Biomater Sci Polym Ed 2009, 20, 2117.
10. Ma, M.; Hill, R. M.; Rutledge, G. C. J Adhes Sci Technol 2008, 22, 1799.
11. Li, D.; Wang, Y. L.; Xia, Y. N. Adv Mater 2004, 16, 361.
12. Bunyan, N. N.; Chen, J.; Chen, I.; Farboodmanesh, S. In: Polymeric Nanofibers (ACS Symposium Series 918); Darrel, H. R., Hao, F., Eds.; American Chemical Society, Washington, DC, 2006; Chapter 8.
13. Katta, P.; Alessandro, M.; Ramsier, R. D.; Chase, G. G. Nano Lett 2004, 4, 2215.
14. Boland, E. D.; Wnek, G. E.; Simpson, D. G.; Pawlowski, K. J.; Bowlin, G. L. J Macromol Sci Pure Appl Chem 2001, 38, 1231.
15. Chew, S. Y.; Wen, J.; Yim, E. K. F.; Leong, K. W. Biomacromolecules 2005, 6, 2017.
16. Song, B.; Cui, W.; Chang, J. J Appl Polym Sci 2011, 122, 1047.
17. Theron, A.; Zussman, E.; Yarin, A. L. Nanotechnology 2001, 12, 384.
18. Zussman, E.; Rittel, D.; Yarin, A. L. Appl Phys Lett 2003, 82, 3958.
19. Yang, F.; Murugan, R.; Wang, S.; Ramakrishna, S. Biomaterials 2005, 26, 2603.
20. Sundaray, B.; Subramanian, V.; Natarajan, T. S.; Xiang, R. Z.; Chang, C. C.; Fann, W. S. Appl Phys Lett 2004, 84, 1222.
21. Tong, H. W.; Wang, M. J Nanosci Nanotechnol 2007, 7, 3834.
22. Teo, W. E.; Kotaki, M.; Mo, X. M.; Ramakrishna, S. Nanotechnology 2005, 16, 918.
23. Kim, K. W.; Lee, K. H.; Khil, M. S.; Ho, Y. S.; Kim, H. Y. Fibers Polym 2004, 5, 122.
24. Gaumer, J.; Prasad, A.; Lee, D.; Lannutti, J. Acta Biomater 2009, 5, 1552.
25. Blond, D.; Walshe, W.; Young, K.; Blighe, F. M.; Khan, U.; Almecija, D.; Carpenter, L.; McCauley, J.; Blau, W. J.; Coleman, J. N. Adv Funct Mater 2008, 18, 2618.
26. Na, H.; Li, Q.; Sun, H.; Zhao, C.; Yuan, X. Polym Eng Sci 2009, 49, 1291.
27. McClure, M. J.; Sell, S. A.; Ayres, C. E.; Simpson, D. G.; Bowlin, G. L. Biomed Mater 2009, 4, 1.
28. Park, H.; Kim, K.; Kim, S. J Aerosol Sci 2004, 35, 1295.
29. Fridrikh, S. V.; Yu, J. H.; Brenner, M. P.; Rutledge, G. C. Phys Rev Lett 2003, 90, 144502.
30. Jaworek, A. J Mater Sci 2007, 42, 266.
31. Mathew, G.; Hong, J. P.; Rhee, J. M.; Leo, D. J.; Nah, C. J Appl Polym Sci 2006, 101, 2017.
32. Sutasinpromprae, J.; Jitjaicham, S.; Nithitanakul, M.; Meechaisue, C.; Supaphol, P. Polym Int 2006, 55, 825.
33. Moon, S.; Farris, R. J. Polym Eng Sci 2007, 47, 1530.
34. Larsen, G.; Spretz, R.; Velarde-Ortiz, R. Adv Mater 2004, 16, 166.
35. Dierich, M.; Gersten, K.; Schlottmann, F. Exp Fluids 1998, 25, 455.
36. Pai, C. L.; Boyce, M. C.; Rutledge, G. C. Macromolecules 2009, 42, 2102.
37. Demir, M. M. eXPRESS Polym Lett 2010, 4, 2.